Advanced Voltage Support And Active Power Flow Control In Grid-Connected Converters Under Unbalanced Conditions

M.Saritha [1], S.Lakshmi Devi [2]
[2] Assoc. Professor
[1, 2] SVPCET

Abstract- *Supporting the grid and improving its reliability have recently become major requirements for large distributed genera- tion units. Under most grid faults, the accuracy of the traditional voltage support schemes (VSSs) is dramatically affected due to the existence of the zero-sequence voltage. Also, the traditional VSSs have been used only in the STATCOM applications, where the ac- tive power is zero. This paper proposes an advanced VSS in the converter-interfaced units, called zero-sequence compensated volt- age support (ZCVS), to accurately regulate the three-phase volt- ages of the connection point within the pre-set safety limits. The proposed scheme not only compensates the zero-sequence com- ponent but also considers the active power injection. Unlike the traditional methods, the proposed VSS is adapted even in resistive distribution systems. The contribution of this paper is, however, ternate. As the second contribution, the limited active power os- cillation (LAPO) is proposed to be augmented to the ZCVS. This feature limits the oscillation to a specified value which provides an adjustable dc-link voltage oscillation setting while simultaneously supporting the ac host grid, even under severe unbalanced faults. Third, the maximum active power delivery (MAPD) to the ac grid is also formulated for the ZCVS. The successful results of the pro- posed support scheme and complementary strategies are verified using selected simulation and experimental test cases.*

Keywords- Active power oscillations, dc voltage ripples, fault ride through, low-voltage ride-through (LVRT) grid codes, maxi- mum power delivery, positive and negative sequence control, reac- tive current injection, unbalanced grid voltages.

I. INTRODUCTION

Pdistributed energy resources to power grids. The safe and proper operation of the grid-connected converters (GCCs) has thus been a substantial challenge for network operators .

This becomes more challenging under various fault conditions. The blend of rising distributed energy resources with large ap- plications of modern loads causes a grid to be more vulnerable to voltage sags, swells, and unbalanced conditions . These distant grid faults can harm the operation of a GCC and, if not controlled properly, cause disastrous cascading failure. How- ever, a GCC can be smartly controlled for not only withstanding these distant faults, but also rendering local ancillary services .

Different control strategies, which are mainly based on sym- metric sequences, were studied to ride through grid faults by a GCC . Each of these studies pursues particular ob- jectives related to the quality of the injected current , dc- voltage ripple reduction, voltage profile regula- tion, or maximum allowable voltage/frequency support . In, multiple objectives, such as mini- mized fault currents, minimized power oscillations, and maxi-mized power flows, are addressed with analytical expressions of the controlling parameters of a GCC under unbalanced faults.

Two control techniques for the static synchronous compensators (STATCOMs) to regulate the positive and negative sequences of the point of common coupling (PCC) voltage, where the ac- tive power delivery is considered zero, are studied in and . In the existing literature, little work has been

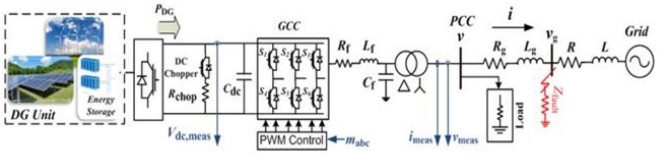

Fig. 1. Circuit topology of the GCC.

carried out on the phase voltage regulation of a GCC under un- balanced conditions. However, the methods presented in [5] and [20] have three drawbacks.

First, they do not consider the zero-sequence voltage compo- nent whereas it exists in most unbalanced faults. Their accuracy are thus severely affected by the zero-sequence component of the PCC voltage, which will be shown later in this paper. Sec- ond, these methods have been only applied in inductive grids, i.e., assuming very high X/R ratio. Third, all of the existing strategies are formulated assuming zero active power delivery.

This paper proposes an advanced voltage support scheme (VSS) addressing these three issues. First, it fully compensates the zero-sequence component and accurately regulates the phase voltages within the preset safety limits under unbalanced fault conditions. The safety voltage limits are typically imposed by grid codes for uninterrupted operation of GCCs. Second, the proposed scheme is applicable to resistive grids, e.g., typical distribution systems. Third, the active power transferred by the GCC is also considered in the proposed VSS. The delivered active power is, however, highly oscillatory under severe un- balanced conditions. This paper also proposes an analytical technique to limit the active power oscillations and enhance dc-bus voltage stabilization, called limited active power oscil- lation (LAPO). As the third contribution, the maximum active power delivery (MAPD) is also formulated. Both of these strate- gies, i.e., LAPO and MAPD, can be simultaneously applied with the proposed VSS. The mathematical equations of the proposed control schemes under various fault conditions are presented in Sections III and IV. The effectiveness of the obtained analytical expressions are validated by selected simulation and experimen- tal test cases in Sections V and VI. Discussions and conclusions are presented in Sections VII and VIII.

II. OPERATION OF A GCC UNDER UNBALANCED CONDITIONS

Fig. 1 illustrates the schematic of a GCC-based DG unit along with its different control parameters. A grid fault or unbalanced loading can cause unbalanced voltage condition at the PCC of a GCC. For any unbalanced condition, the positive and negative- sequence voltage vectors can be written in the αβ frame as

$$v^{\pm} = \begin{matrix} v_\alpha^+ \\ v_\beta^+ \end{matrix} = \begin{matrix} V_+ \cos(\omega t + \delta_+) \\ V_+ \sin(\omega t + \delta_+) \end{matrix}$$

$$v^{-} = \begin{matrix} v_\alpha^- \\ v_\beta \end{matrix} \quad \begin{matrix} V_- \cos(\omega t + \delta_-) \\ -V_- \sin(\omega t + \delta_-) \end{matrix}$$

To exploit a flexible supportive performance from a GCC, its injected current vector i can be divided into four vectors of posi- tive and negative sequences and active and reactive components as

$$i = i_{p+} + i_{p-} + i_{q+} + i_{q-}$$

$$i = \begin{matrix} i_\alpha \\ i_\beta \end{matrix} = \begin{matrix} I_{p+}\cos(\omega t + \delta_+) + I_{p-}\cos(\omega t + \delta_-) \\ I_{p+}\sin(\omega t + \delta_+) - I_{p-}\sin(\omega t + \delta_-) \end{matrix} + \begin{matrix} I_{q+}\sin(\omega t + \delta_+) - I_{q-}\sin(\omega t + \delta_-) \\ -I_{q+}\cos(\omega t + \delta_+) - I_{q-}\cos(\omega t + \delta_-) \end{matrix} \quad (2)$$

where the superscripts "+"/"-" and subscripts "p"/"q" denote the positive/negative and active/reactive components, respectively.

These current components should be found in a way that they can provide the required voltage support with any grid condition.

The mathematical expressions of the ac-side voltages in terms of the injected active/reactive currents are as

$$v = v_+ + v_- = \begin{matrix} v_\alpha^+ + v_\alpha^- \\ v_\beta + v_\beta^- \end{matrix} = \begin{bmatrix} v_{g\alpha}^+ + v_{g\alpha}^- + L_g \dfrac{di_\alpha}{dt} + R_g i_\alpha \\ v_{g\beta}^+ + v_{g\beta}^- + L_g \dfrac{di_\beta}{dt} + R_g i_\beta \end{bmatrix} \quad (3)$$

where the subscript "g" represents the grid components accord-ing to Fig. 1. Equation (3) can be expanded as

$$\begin{matrix} V_+\cos(\omega t + \delta_+) + V_-\cos(\omega t + \delta_-) \\ V_+\sin(\omega t + \delta_+) - V_-\sin(\omega t + \delta_-) \end{matrix} = \begin{matrix} V_{g+}\cos(\omega t + \delta_{g+}) + V_{g-}\cos(\omega t + \delta_{g-}) \\ V_{g+}\sin(\omega t + \delta_{g+}) - V_{g-}\sin(\omega t + \delta_{g-}) \end{matrix}$$

$$+ L_g\omega \begin{matrix} I_{q+}\cos(\omega t + \delta_+) - I_{q-}\cos(\omega t + \delta_-) \\ I_{q+}\sin(\omega t + \delta_+) + I_{q-}\sin(\omega t + \delta_-) \end{matrix} + L_g\omega \begin{matrix} -I_{p+}\sin(\omega t + \delta_+) - I_{p-}\sin(\omega t + \delta_-) \\ I_{p+}\cos(\omega t + \delta_+) - I_{p-}\cos(\omega t + \delta_-) \end{matrix}$$

$$+ R_g \begin{matrix} I_{p+}\cos(\omega t + \delta_+) + I_{p-}\cos(\omega t + \delta_-) \\ I_{p+}\sin(\omega t + \delta_+) - I_{p-}\sin(\omega t + \delta_-) \end{matrix} + R_g \begin{matrix} I_{q+}\sin(\omega t + \delta_+) - I_{q-}\sin(\omega t + \delta_-) \\ -I_{q+}\cos(\omega t + \delta_+) - I_{q-}\cos(\omega t + \delta_-) \end{matrix} \quad (4)$$

In general, the difference between δ + and δg is negligible. Therefore, the analytical solution of the problem

can be simpli- fied by assuming δ + and δg to be equal. Equation (4) can be represented as

$$\begin{aligned} &V_{+} - V_{g+}\cos(\omega t + \delta_{+}) + V_{-} - V_{g-}\cos(\omega t + \delta_{-}) \\ &V_{+} - V_{g+}\sin(\omega t + \delta_{+}) - V_{-} - V_{g-}\sin(\omega t + \delta_{-}) \end{aligned}$$

$$= \begin{bmatrix} L_g \omega I_q^{+} + R_g I_p \cos(\omega t + \delta_{+}) \\ L_g \omega I_q^{+} + R_g I_p \sin(\omega t + \delta_{+}) \end{bmatrix} + \begin{bmatrix} R_g I_p - L_g \omega I_q \cos(\omega t + \delta_{-}) \\ -R_g I_p - L_g \omega I_q \sin(\omega t + \delta_{-}) \end{bmatrix} \quad (5)$$

if the following expressions are satisfied:

$$\frac{I_p^{+}}{I_q^{+}} = \frac{R_g}{L_g \omega}, \quad \frac{I_p^{-}}{I_q^{-}} = -\frac{R_g}{L_g \omega}. \quad (6)$$

Then, the positive and negative components of (5) result in

$$\begin{aligned} V_{+} - V_{g+} &= L_g \omega I_q + R_g I_p \\ V_{-} - V_{g-} &= R_g I_p - L_g \omega I_q \end{aligned} \quad (7)$$

III. PROPOSED ZERO-SEQUENCE COMPENSATED VOLTAGE SUPPORT (ZCVS) SCHEME

The basic requirement in the voltage support is to avoid the over-voltage and under-voltage at the PCC whenever possible. If the rated power of the GCC and the connecting line impedance are not small, the three-phase voltages can be regulated at the preset safety limits, i.e., V_{min}^{set} and V_{max}^{set}. In this paper, the proposed scheme was only applied to the STATCOM application where the reference current only consists of the reactive components. However, the effect of the active power in regulating the volt- age should not be ignored at the distribution level since: the resistance of the lines in the distribution system is not negligi- ble; and DGs inherently generate and inject the active power to the system. Therefore, the active components of the current are also taken into account in this paper as presented in the follow- ing section. Complying with voltage limits during unbalanced grid faults, the maximum and minimum phase voltages should respect

$$\begin{aligned} V_{max} &= \max\{V_a, V_b, V_c\} \le V_{max}^{set} \\ V_{min} &= \min\{V_a, V_b, V_c\} \ge V_{min}^{set} \end{aligned} \quad (8)$$

where Va , Vb , and Vc are the magnitude of the three-phase volt- set set ages at the PCC of the GCC. The value of Vm in – Vm ax are set to 0.9–1.1 p.u. and 0.8–1.2 p.u., respectively, in the simulation and experimental tests in this paper. To meet these limits, a combi- + nation of positive/negative and active/reactive currents (i.e., Ip , −+ − Ip , Iq , and Iq) should be injected into an inductive or resistive grid to support the grid voltage. These four reference values should be properly found such that the maximum phase volt- set age does not overpass Vm ax , and the minimum phase voltage is set kept at (or above) Vm in . The ac-side VSS can be extracted as a function of the grid voltage and the injected positive/negative currents. The magnitudes of the phase voltages can be obtained in terms of the magnitudes of positive and negative sequence voltages by the following expressions:

$$\begin{cases} V_a = \sqrt{(V_+)^2 + (V_-)^2 + 2(V_+)(V_-)\cos(\gamma) + V_0 \cos\gamma_0} \\ V_b = \sqrt{(V_+)^2 + (V_-)^2 + 2(V_+)(V_-)\cos\left(\gamma - \frac{2\pi}{3}\right) + V_0 \cos\left(\gamma_0 - \frac{2\pi}{3}\right)} \\ V_c = \sqrt{(V_+)^2 + (V_-)^2 + 2(V_+)(V_-)\cos\left(\gamma + \frac{2\pi}{3}\right) + V_0 \cos\left(\gamma_0 + \frac{2\pi}{3}\right)} \end{cases} \quad (9)$$

where $\gamma = \delta_+ - \delta_-$ and $\gamma_0 = \delta_0 - \delta_+$. From (9), the maximum and minimum phase voltages can be determined by

$$\begin{aligned} V_{min} &= \min(V_a, V_b, V_c) \\ &= \sqrt{(V_+)^2 + (V_-)^2 + 2(V_+)(V_-)\lambda_{min} + V_0 \lambda_{0\,min}} \\ V_{max} &= \max(V_a, V_b, V_c) \\ &= \sqrt{(V_+)^2 + (V_-)^2 + 2(V_+)(V_-)\lambda_{max} + V_0 \lambda_{0\,max}} \end{aligned} \quad (10)$$

where λmin , λmax , λ0 in , and λ0 ax can be found as follows:

$$\begin{cases} \lambda_a = \cos(\gamma) \\ \lambda_b = \cos\left(\gamma - \frac{2\pi}{3}\right) \\ \lambda_c = \cos\left(\gamma + \frac{2\pi}{3}\right) \end{cases} \rightarrow \begin{aligned} \lambda_{min} &= \min(\lambda_a, \lambda_b, \lambda_c) \\ \lambda_{max} &= \max(\lambda_a, \lambda_b, \lambda_c) \end{aligned}$$

$$\begin{cases} \text{if } \lambda_{min} = \lambda_a \rightarrow \lambda_{0\,min} = \cos\gamma_0 \\ \text{if } \lambda_{min} = \lambda_b \rightarrow \lambda_{0\,min} = \cos\left(\gamma_0 - \frac{2\pi}{3}\right) \\ \text{if } \lambda_{min} = \lambda_c \rightarrow \lambda_{0\,min} = \cos\left(\gamma_0 + \frac{2\pi}{3}\right) \end{cases}$$

$$\text{and} \quad \begin{cases} \text{if } \lambda_{max} = \lambda_a \rightarrow \lambda_{0\,max} = \cos\gamma_0 \\ \text{if } \lambda_{max} = \lambda_b \rightarrow \lambda_{0\,max} = \cos\left(\gamma_0 - \frac{2\pi}{3}\right) \\ \text{if } \lambda_{max} = \lambda_c \rightarrow \lambda_{0\,max} = \cos\left(\gamma_0 + \frac{2\pi}{3}\right) \end{cases} \quad (11)$$

The reference values for the maximum and minimum phase voltages of (10) can be determined such that the phase voltages are regulated within the explained thresholds of (8). This can be accomplished by setting the reference values as

$$V_{m\,in}^{ref} = V_{m\,in}^{set}$$
$$V_{m\,ax}^{ref} = \min(V_{m\,ax}^{set}, (V_{m\,ax} - V_{m\,in})). \quad (12)$$

After finding the proper Vm in and Vm ax by (12) and applying +them in (10), the reference values for the Vref and Vref can be solved as

$$V_{ref}^{+\,2} = \frac{-B + \sqrt{B_2 - 4A_2}}{2}$$
$$V_{ref}^{-} = \frac{A}{V_{ref}^{+}} \quad (13)$$

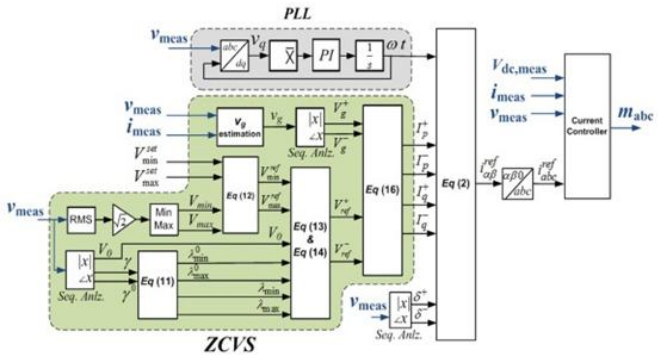

Fig. 2. Proposed VSS

where

$$\begin{cases} A = \dfrac{V_H^{+} - V_L^{+\,2}}{2(\lambda_{m\,ax} - \lambda_{m\,in})} \\ B = 2A \times \lambda_{m\,ax} - V_H^{+\,2} \end{cases}$$
$$V_L = V_{m\,in}^{set} - V_0 \lambda_{0\,in_m}$$
$$V_H = V_{m\,ax}^{set} - V_0 \lambda_{0\,ax_m} \quad (14)$$

Using (13) and (14), the reference values for the desired positive and negative sequences of the voltage are obtained. Then, V + and V − in (7) are replaced with the reference values obtained by (13) and (14). Moreover, Vg+ and Vg− can be esti- mated by using the PCC measurements. Therefore, (7) can be rewritten as

$$\begin{matrix} \Delta V_{ref}^{+} \\ \Delta V_{ref}^{-} \end{matrix} = \begin{matrix} \omega L_g I_q^{+} \\ -\omega L_g I_q^{-} \end{matrix} + \begin{matrix} R_g I_p^{+} \\ R_g I_p^{-} \end{matrix}. \quad (15)$$

Now, the solution of (15) exists in the determination of fourB current components (Ip , Ip , Iq , and Iq). A general solution for (15), which is applicable in grids with any X/R ratio, can be obtained as

$$I_p^{+} = \frac{R_g}{X_g^{2} + R_g^{2}} \times \Delta V_{ref}^{+}, \quad I_p^{-} = \frac{R_g}{X_g^{2} + R_g^{2}} \times \Delta V_{ref}^{-}$$
$$I_q^{+} = \frac{X_g}{X_g^{2} + R_g^{2}} \times \Delta V_{ref}^{+}, \quad I_q^{-} = \frac{-X_g}{X_g^{2} + R_g^{2}} \times \Delta V_{ref}^{-} \quad (16)$$

where expressions of (6) are also satisfied. In inductive and resistive grids, the effective current components in providing voltage support can be conducted from (16), respectively, as

$$I_q^{+} = \frac{\Delta V_{ref}^{+}}{X}, \quad I_q^{-} = \frac{-\Delta V_{ref}^{-}}{X} \quad (17)$$

And

$$I_p^{+} = \frac{\Delta V_{ref}^{+}}{R}, \quad I_p^{-} = \frac{\Delta V_{ref}^{-}}{R}. \quad (18)$$

IV. PROPOSED COMPLEMENTARY STRATEGIES

In the previous section, the positive and negative sequences of the reactive current component were obtained for regulat- ing the phase voltages in an inductive grid. In this section, two complementary strategies are proposed to be applied to the ac- tive and reactive components of the current. The first strategy, i.e., LAPO, aims to limit the oscillations on the active power, which is critical to improve the dc-bus voltage stabilization. Furthermore, the second strategy, i.e., MAPD, intends to deliver the maximum active power with respect to the rating current while simultaneously supporting the voltage with ZCVS. These strategies can also be obtained for the resistive grids and grids with any X/R value if the active and reactive components are replaced or (6) is satisfied.

A. ZCVS With LAPO Strategy

In severe unbalanced conditions, the required negative reac- tive component of the current obtained by ZCVS may become high. Negative-sequence current and voltage components give rise to large oscillations in the active power. Therefore, the LAPO strategy is proposed to obtain a limit for the negative re- active current component, which does not cause exceeding the ˜ set preset maximum allowable active power oscillation Pm ax . Con- sidering the symmetric-sequence-based instantaneous power

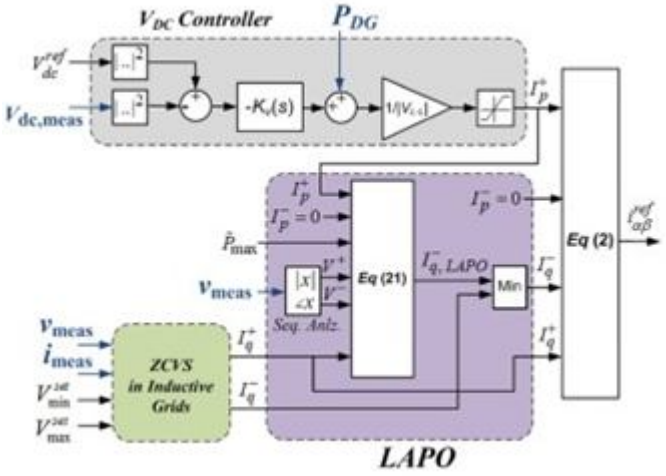

Fig. 3. Proposed control diagram to limit the active power oscillations

theory, the output active power of the GCC is calculated as follows [24]–[25]:

$$p = v.\ i = (v_+ + v_-).(i_+ + i_-)$$
$$= v_+.\ i_+ + v_-.\ i_- + v_+.\ i_- + v_-.\ i_+. \quad (19)$$

Using the corresponding equivalents of the positive/negative voltage and current vectors from (1) and (2) give the magnitude of the oscillations on the active power as

$$\tilde{P} = \sqrt{V_- I_p + V_+ I_p}^{\,2} + \sqrt{V_- I_q - V_+ I_q}^{\,2} \quad (20)$$

Using (20), the equation of the maximum negative reactive current will be obtained, which limits the oscillation magnitude ˜ set of the active power to Pm ax :

$$I_{q,LAPO}^{-} = \frac{\sqrt{P_{set2} - V_- I_p + V_+ I_p}^{\,2} + V_- I_q}{V_+}. \quad (21)$$

This analytical expression limits the active power oscilla- tions and enhances the dc-bus voltage stabilization. Fig. 3 shows the control diagram of the ZCVS scheme with LAPO strategy. LAPO may slightly affect the operation of the ZCVS. How- ever, the GCC operator can flexibly compromise between the full ZCVS and the LAPO capability, by using these analytical expressions.

B. ZCVS With MAPD Strategy

Applying the MAPD technique ensures delivering the max- imum allowable active power to the grid and simultaneously respecting the current limitations while riding through abnor- mal conditions, and simultaneously regulating the phase volt- + ages. Therefore, this section finds the equation of Ip,M APD to + achieve the aforementioned goals. Ip,M APD is the term deter- + mining the maximum allowable value for Ip to provide the maximum allowable active power injection such that none of set + − the phase currents passes Im ax . In this strategy, Iq and Iq are already obtained by (17) to provide the proposed voltage

support. The value of I_p is also set to zero to allocate all the available current capacity to I_p . Then, (2) can be rewritten as

$$\begin{bmatrix} i_\alpha \\ i_\beta \end{bmatrix} = \begin{bmatrix} I_p \cos(\omega t + \delta_+) + I_q \sin(\omega t + \delta_+) - I_q \sin(\omega t + \delta_-) \\ I_p \sin(\omega t + \delta_+) - I_q \cos(\omega t + \delta_+) - I_q \cos(\omega t + \delta_-) \end{bmatrix} \quad (22)$$

$$\begin{bmatrix} i_\alpha \\ i_\beta \end{bmatrix} = \begin{bmatrix} I_p^+ + I_q \sin\gamma \cos(\omega t + \delta_+) + I_q - I_q \cos\gamma \sin(\omega t + \delta_-) \\ I_p^- - I_q \sin\gamma \sin(\omega t + \delta_+) - I_q + I_q \cos\gamma \cos(\omega t + \delta_-) \end{bmatrix} \quad (23)$$

The αβ currents of (23) are transformed into the abc currents, and the magnitude of the phase currents will be obtained as

$$\begin{bmatrix} I_a^2 \\ I_b^2 \\ I_c^2 \end{bmatrix} = \begin{bmatrix} (I_{ac})^2 + (I_{as})^2 \\ \left(-\frac{1}{2} I_{ac} + \frac{\sqrt{3}}{2} I_{as}\right)^2 + \left(-\frac{\sqrt{3}}{2} I_{ac} - \frac{1}{2} I_{as}\right)^2 \\ \left(-\frac{1}{2} I_{ac} - \frac{\sqrt{3}}{2} I_{as}\right)^2 + \left(\frac{\sqrt{3}}{2} I_{ac} - \frac{1}{2} I_{as}\right)^2 \end{bmatrix} \quad (24)$$

where

$$\begin{cases} I_{ac} = I_p + I_q \sin\gamma \\ I_{as} = I_+ \cos - I_q \cos\gamma \\ I_{bs} = I_p - I_q \sin\gamma \\ I_{bc} = -I_q + I_q \cos\gamma \end{cases} \quad (25)$$

Then, the phase current magnitudes under the fault can be found by

$$I_a^2 = I_p + I_q \sin\gamma^{-} \;^2 + I_q - I_q \cos\gamma \;^2 \quad (26)$$

$$I_b^2 = \left(-\frac{1}{2} I_p + I_q \sin\gamma - \frac{\sqrt{3}}{2} I_q + I_q \cos\gamma\right)^2 + \left(-\frac{1}{2} I_q \cos\gamma + \frac{\sqrt{3}}{2} I_p - I_q \sin\gamma\right)^2$$
$$= \left(\frac{1}{2} I_{a1} + I_{a2}\right)^2 + \left(\frac{\sqrt{3}}{2} I_{a1} + I_{a2}\right)^2 \quad (27)$$

$$I_c^2 = \left(-\frac{1}{2} I_p + I_q \sin\gamma + \frac{\sqrt{3}}{2} I_q + I_q \cos\gamma\right)^2 + \left(-\frac{1}{2} I_q \cos\gamma - \frac{\sqrt{3}}{2} I_p - I_q \sin\gamma\right)^2$$
$$= \left(\frac{1}{2} I_{a3} + I_{a4}\right)^2 + \left(-\frac{\sqrt{3}}{2} I_{a3} + I_{a4}\right)^2 \quad (28)$$

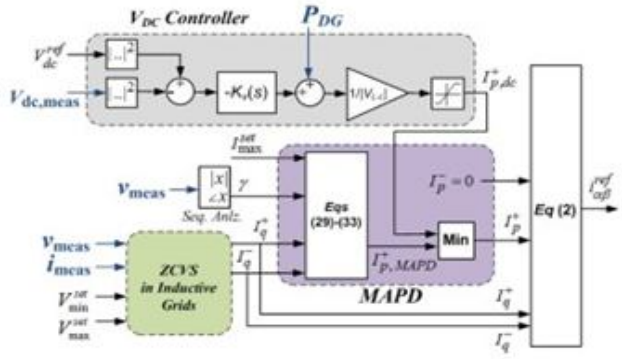

Fig. 4. shows the control diagram of the ZCVS scheme with MAPD strategy.

where

$$I_{q1} = I_q \sin\gamma + \frac{\sqrt{3}}{2} I_q + \frac{\sqrt{3}}{2} I \cos\gamma$$

$$I_{q2} = -I_q \frac{1}{2} I_q \frac{1}{2} \cos\gamma - \frac{\sqrt{3}}{2} I \sin\gamma$$

$$I_{q3} = I_q \sin\gamma - \frac{\sqrt{3}}{2} I_q - \frac{\sqrt{3}}{2} I \cos\gamma$$

$$I_{q4} = -I_q \frac{1}{2} I_q \frac{1}{2} \cos\gamma + \frac{\sqrt{3}}{2} I \sin\gamma. \quad (29)$$

Using (26)–(29), three values are, respectively, obtained for I_D ($I_{D,a}^+$, $I_{D,a}^-$, and $I_{D,c}^-$) in three cases, i.e., $I_a = I_{max}^{set}$, $I_b = I_{max}^{set}$, and $I_c = I_{max}^{set}$

$$I_{D,a}^- = \sqrt{I_{max2} - I_q - I_q \cos\gamma}^{\,2} - I_q \sin\gamma \quad (30)$$

$$I_{D,b}^- = \frac{-I_{q1} - \sqrt{3} I_{q2} + \sqrt{I_{q1} + \sqrt{3} I_{q2}}^{\,2} - 4 I_{q1}^2 + I_{q2}^2 - I_{max2}^{set}}{2} \quad (31)$$

$$I_{D,c}^- = \frac{-I_{q3} + \sqrt{3} I_{q4} + \sqrt{I_{q3} - \sqrt{3} I_{q4}}^{\,2} - 4 I_{q3}^2 + I_{q4}^2 - I_{max2}^{set}}{2} \quad (32)$$

$$I_{D,MAPD}^- = \min I_{D,a}^-, I_{D,b}^-, I_{D,c}^-. \quad (33)$$

V. SIMULATION RESULTS

To demonstrate the effectiveness of the proposed ZCVS scheme with LAPO and MAPD strategies, three test cases are studied and implemented in this paper. Fig. 1 illustrates the circuit topology of a grid-connected 1.0 MVA, 690 V, 60 Hz converter-interfaced DG unit. The operation of a GCC under the unbalanced ac-side condition is usually studied by assuming a

TABLE I
TEST SYSTEM PARAMETERS

Z_g (Test A)	0.3 Ω	V_{dc}	2000 V
Z_g (Test B-LAPO)	0.3 Ω	$V_{L-L,RMS}$	690 V
Z_g (Test B-MAPD)	0.15 Ω	f	60 Hz
Z_g (Test C-Resistive)	0.3 Ω	S	1.0 MVA
Z_g (Test C-X/R = 1)	0.21 + j 0.21 Ω	I_{max}	200 A
$V_{sag} = V_{1(min)}$	0.9 p.u.	$V_{swell} = V_{1(max)}$	1.1 p.u.

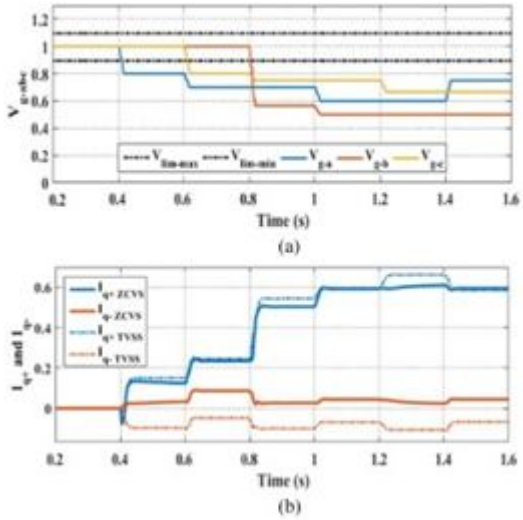

Fig. 5. Simulation test case A: (a) magnitudes of the grid phase voltages, and (b) obtained positive and negative reactive currents by TVSS and ZCVS.

constant dc voltage source in the dc-side for simplicity. This is a common assumption in most studies (e.g., in [2], [5], [14]– [15], [22]–[26]). To realistically emulate a renewable energy resource, the dc voltage regulator is used in this paper. There- fore, the dc-link voltage controller generates the active power command of the GCC. The simulation system parameters are listed in Table I.

A. Test Case A: Traditional VSS Versus Proposed ZCVS Method

This section presents the simulation results of the tradi- tional voltage support scheme (TVSS) and the proposed ZCVS method. Fig. 5(a) shows six different unbalanced faulty condi- tions. Between t = 0.4 s and t = 0.6 s, a single-phase fault happens on phase A (i.e., the magnitude of phase A is decreased to 0.8 p.u.). From t = 0.6 s, each phase voltage experiences different sags to show and compare the performances of the traditional and proposed methods. For example, the magnitudes of phase voltages a, b, and c are, respectively, 0.6, 0.5, and 0.75 p.u. between t = 1 s and t = 1.2 s. Fig. 5(b) indicates the + − obtained Iq and Iq by the TVSS and ZCVS for different fault conditions. As Fig. 6(a)-left reveals, TVSS fails to precisely regulate the phase voltages within the preset voltage limits. Over-voltages up to 1.18 p.u.

(on phase B between t = 0.6 s and t = 0.8 s) and under-voltages down to 0.83 p.u. (on phase

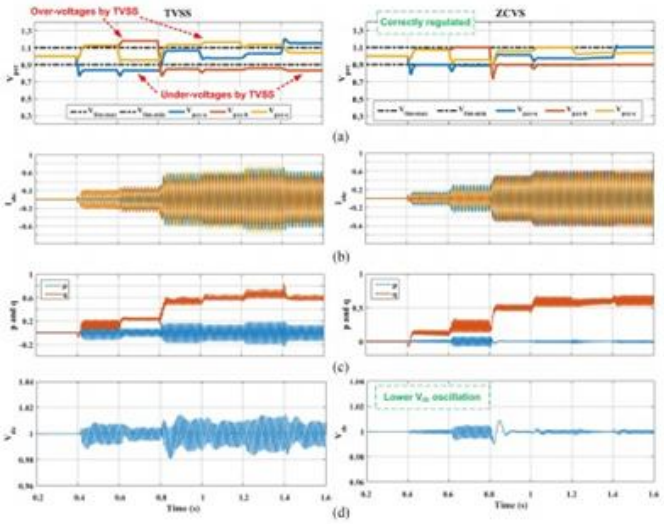

Fig. 6. Simulation results of the traditional (left side) and proposed (right side) voltage support methods: (a) magnitudes of the PCC phase voltages, (b) phasecurrents, (c) active and reactive powers, and (d) dc voltage.

A between t = 0.4 s and 0.8 s and on phase B between t = 1.4 s and t = 1.6 s) occur whereas the voltage accepted limits are set to ±0.1 p.u. around the nominal value. However, the proposed ZCVS method demonstrates successful results. As Fig. 6(a)-right shows, the phase-voltages of the PCC are pre- set set cisely regulated between the Vm in and Vm ax . Also, it is notable from Fig. 6(d) that the dc voltage ripples are considerably lower when the ZCVS is applied.

B. Test Case B: ZCVS Method With LAPO and MAPD Strategies

First, the result of the ZCVS method with LAPO strategy is presented. The maximum acceptable oscillation on the active − power is set to 0.08 p.u. Using (21), the maximum Iq is calcu- lated where the active power oscillations are lower than 0.08 p.u. − As Fig. 7(a) demonstrates, the Iq calculated by (17) is higher − than Iq ,LAPO . It causes active power oscillations greater than − 0.08 p.u., as depicted in Fig. 7(c). To limit the oscillations, Iq − is limited to Iq ,LAPO at t = 0.5 s and t = 0.9 s, as indicated in Fig. 7(a). Therefore, the active power oscillations are limited to 0.08 p.u., as shown in Fig. 7(c). As a result, the dc voltage ripples are decreased by applying LAPO strategy.\

As another complementary strategy, the ZCVS method with set MAPD strategy is tested in this section. The value of Im ax is set to 1.0 p.u. Using (29)–(33), the suitable Ip is calculated such that set all phase currents are limited to Im ax . Fig. 8(a) shows that an unbalanced fault occurs at t = 0.3 s. The prefault active power is 1 p.u., which causes overcurrent, as Fig. 8 illustrates. At t = 0.5 s the chopper in the dc-side is activated to avoid the overcurrent, and the delivered active power becomes zero, as indicated in Fig. 8(f). At t = 0.7 s, the active current component obtained by (29)–(33) is applied, as shown in Fig. 8(d). Thus, the MAPD

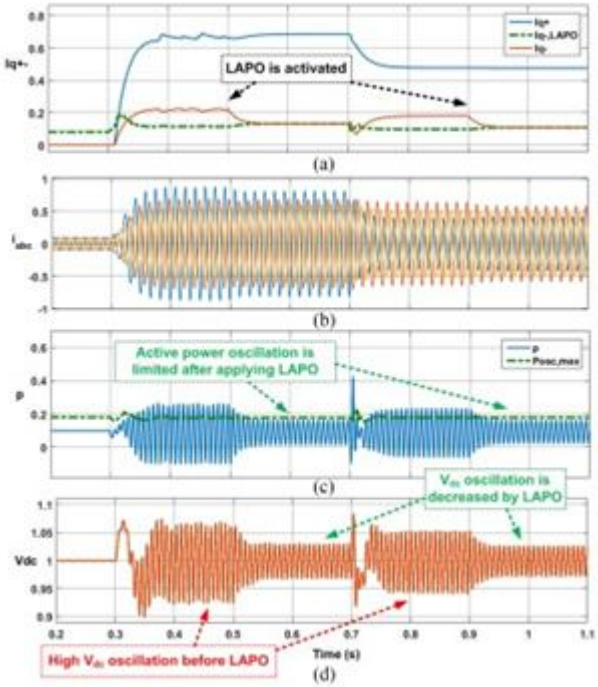

Fig. 7. Simulation results of ZCVS with LAPO strategy: (a) obtained positive and negative reactive currents by ZCVS and LAPO, (b) phase currents, (c) active power, and (d) dc voltage.

strategy allows delivering maximum allowable active power [see Fig. 8(f)] while simultaneously respects the phase current limit [see Fig. 8(e)] under faulted condition. As Fig. 8(b) shows, the

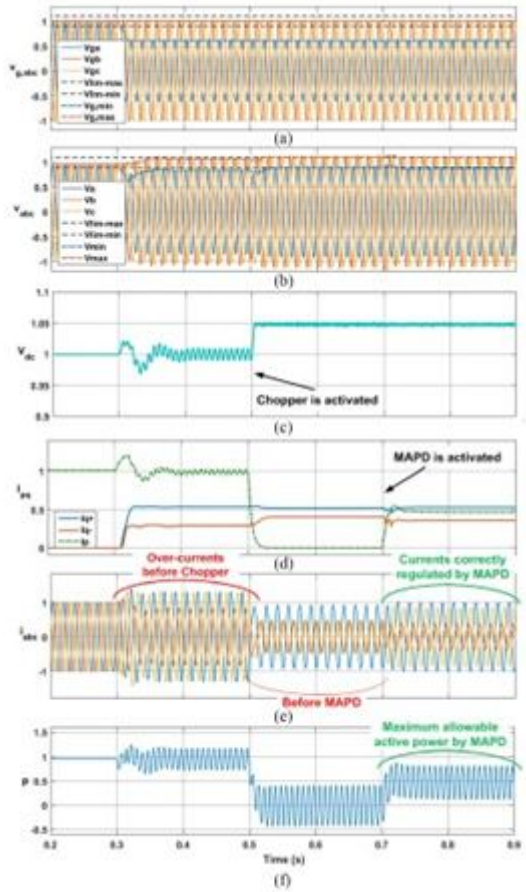

Fig. 8. Simulation results of ZCVS with MAPD strategy: (a) grid phase voltages, (b) PCC phase voltages, (c) dc voltage, (d) active current and positive/negative reactive currents, (e) phase currents, and (f) active power.

TABLE II
EXPERIMENTAL TEST SYSTEM PARAMETERS

Z_0	$\lvert 2\pi f \times 1.2e-3 \rvert\ \Omega$	Grid voltage	110 V
Z	$\lvert 2\pi f \times 2.7e-3 \rvert\ \Omega$	Transformer secondary voltage	17 V
		S	1500 VA
f	60 Hz	$I_{Max} = I_{limit}$	20 A
k_{p-PLL}	200	k_{I-PLL}	4000
$V_{Min} = V_{limit}$	20 V	$V_{Max} = V_{limit}$	30 V

ZCVS is still operating accurately even if the MAPD strategy is applied.

C. Test Case C: ZCVS Method Under Various X/R Ratios

In the previous test cases, the ZCVS was applied to inductive grids (i.e., X/R >>1). In this test case, the ZCVS is tested in two other systems: a resistive grid (i.e., X/R ≈ 0) and a grid with X/R = 1. Figs. 9 and 10 demonstrate the successful results of the ZCVS in regulating the phase voltages in these two cases. As Fig. 9(a) reveals, the ZCVS uses only the active current component in positive and negative sequences in

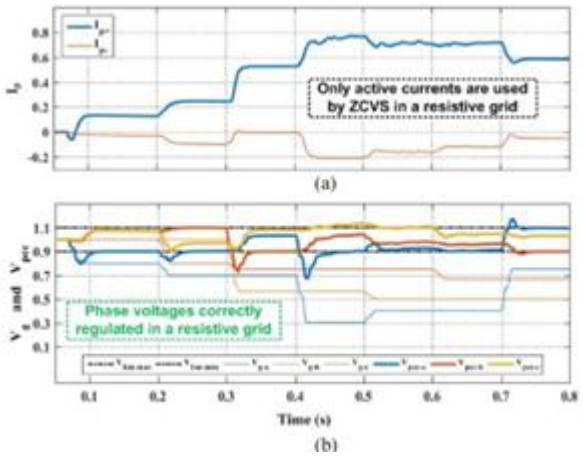

Fig. 9. Simulation results of ZCVS in a resistive grid: (a) positive and negative active currents, (b) magnitudes of grid and PCC phase voltages.

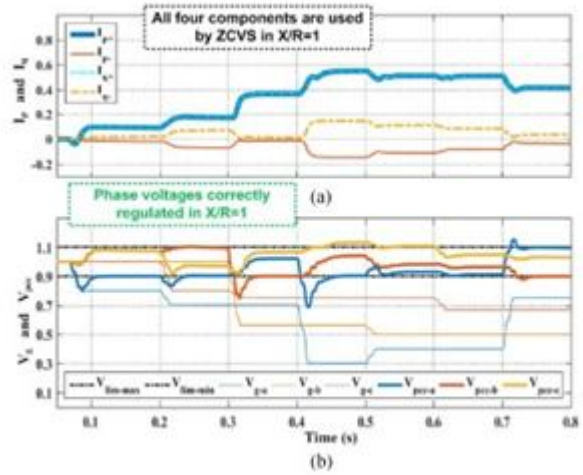

Fig. 10. Simulation results of ZCVS in a grid with X/R = 1: (a) positive and negative active currents, (b) magnitudes of grid and PCC phase voltages.

the resistive grid, according to (18). However, in the grid with X/R = 1, both active and reactive currents in positive and neg- ative sequences have been utilized according to (16), as shown in Fig. 10(a).

VI. EXPERIMENTAL RESULTS

To further verify the presented analytical expressions and demonstrate the performance of the proposed ZCVS, the scaled- down test system is also employed. This system contains a voltage-source converter connected to an ac grid via impedances and a transformer. The switching frequency is 10 kHz. Other parameters of the test system are reported in Table II. The converter is interfaced to a dSPACE1104 control card via a CMOS/TTL interfacing circuit. The converter is connected to a 60-Hz, 110-V (phase-voltage) three-phase grid

via three-phase transformer. Using this transformer, the converter-

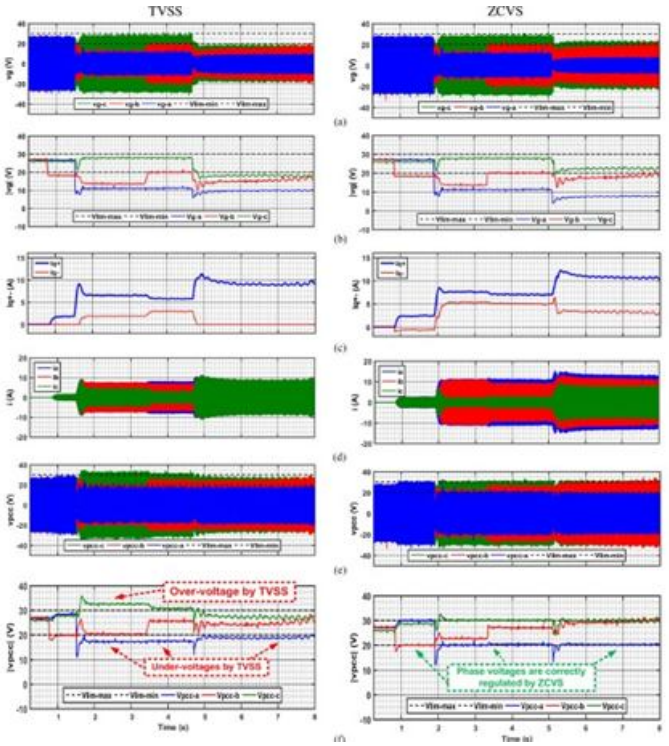

Fig. 11. Experimental test results with traditional and proposed methods, i.e., TVSS (left-side) and ZCVS (right-side): (a) grid phase voltages, (b) magnitudes of the grid phase voltages, (c) obtained reactive currents by TVSS and ZCVS, (d) phase currents, (e) PCC phase voltages, and (f) magnitudes of the PCC phase voltages.

operating voltage is reduced to safely emulate the grid faults and disturbances. The software code is generated by using the real-time toolbox under a MATLAB/Simulink environment. Three proportional-resonant controllers are designed to regulate the current in the abc frame and positive/negative components.

The experimental results of the traditional and proposed meth- ods are obtained under different unbalanced fault conditions and presented in Fig. 11. The unbalanced faults are realized using circuit breakers and different fault impedances for each phase. + − Figs. 11(c) indicate the obtained Iq and Iq by the traditional VSS and ZCVS. As Fig. 11(f)-left reveals, the traditional method fails to precisely regulate the phase voltages within the preset voltage limits. Steady-state over-voltage up to 1.32 p.u. (on phase C between t = 1.8 s and 3.4 s) and under-voltage down to 0.68 p.u. (on phase A between t = 1.8 s and 4.7 s) occur. It is due to neglecting the zero-sequence voltage in the traditional VSS. However, the proposed ZCVS method demonstrates suc- cessful performance and accurate phase voltage regulation, as illustrated in Fig. 11(f)-right.

VII. CONCLUSION

This paper proposes an advanced VSS to precisely regulate the phase voltages of a three-phase GCC within the preset safety limits. Existing methods mainly suffer from three problems: first, their performance becomes inaccurate in most cases be- cause of ignoring the zero-sequence voltage component; second, they can be only applied in inductive grids; and, third, zero ac- tive power delivery is suggested. The proposed ZCVS method addresses these three problems. Moreover, two complementary objectives, related to the active power delivery, are also aug- mented in the proposed scheme. First, the LAPO is proposed under severe unbalanced faults to analytically obtain a limit for the injected negative reactive current. This feature provides an adjustable and limited oscillation on active power, and improved dc voltage while supporting the ac-side voltage. Second, the ex- pressions of the MAPD are proposed to exploit the maximum allowable active power of a distributed energy resource even under severe unbalances and while still regulating the phase voltages. The proposed VSS and two complementary strategies bring significant advantages to emerging distributed generation units. The successful results of the proposed schemes are veri- fied using simulation and experimental tests.

REFERENCES

[1] M. K. Hossain and M. H. Ali, “Transient stability augmentation of PV/DFIG/SG-based hybrid power system by nonlinear control-based variable resistive FCL,” IEEE Trans. Sustain. Energy, vol. 6, no. 4, pp. 1638–1649, Oct. 2015.

[2] H. Xiao, A. Luo, Z. Shuai, G. Jin, and Y. Huang, “An improved con- trol method for multiple bidirectional power converters in hybrid AC/DC microgrid,” IEEE Trans. Smart Grid, vol. 7, no. 1, pp. 340–347, Jan. 2016.

[3] P. Wang, C. Jin, D. Zhu, Y. Tang, P. C. Loh, and F. H. Choo, “Distributed control for autonomous operation of a three-port AC/DC/DS hybrid micro- grid,” IEEE Trans. Ind. Electron., vol. 62, no. 2, pp. 1279–1290, Feb. 2015.

[4] K. A. Alobeidli, M. Syed, M. E. Moursi, and H. Zeineldin, “Novel coor- dinated voltage control for hybrid micro-grid with islanding capability,” IEEE Trans. Smart Grid, vol. 6, no. 3, pp. 1116–1127, May 2015.

[5] A. Camacho, M. Castilla, J. Miret, R. Guzmanm, and A. Borrell, “Reactive power control for distributed generation power plants to comply with voltage limits during grid faults,” IEEE Trans. Power Electron., vol. 29, no. 11, pp. 6224–6234, Nov. 2014.

[6] S. Chaudhary, R. Teodorescu, P. Rodriguez, P. C. Kjaer, and A. M. Gole, "Negative sequence current control in wind power plants with VSC-HVDC connection," IEEE Trans. Sustain. Energy, vol. 3, no. 3, pp. 535–544, Jul. 2012.

[7] Y. Mohamed and E. El-Saadany, "A control scheme for PWM voltage source distributed-generation inverters for fast load-voltage regulation and effective mitigation of unbalanced voltage disturbances," IEEE Trans. Ind. Electron., vol. 55, no. 5, pp. 2072–2084, May 2008.

[8] A. M. Howlader and T. Senjyu, "A comprehensive review of low volt- age ride through capability strategies for the wind energy conversion systems," Renew. Sustain. Energy Rev., vol. 56, pp. 643–658, Apr. 2016.

[9] M. Mohammadalizadeh-Shabestary et al., "A general approach for op- timal allocation of FACTS devices using equivalent impedance models of VSCs" Int. Trans. Electr. Energy Syst., vol. 25, pp. 1187–1203, Jul. 2015.

[10] H. H. Dezaki et al., "A new method based on sensitivity analysis to optimize the placement of SSSCs," Turk. J. Electr. Eng. Comput. Sci., vol. 21, no. 1, pp. 1956–1971, Dec. 2013.

[11] A. K. Pathak, M. P. Sharma, and M. Bundele, "A critical review of voltage and reactive power management of wind farms," Renew. Sustain. Energy Rev., vol. 51, pp. 460–471, Nov. 2015.

[12] M. Nasiri, J. Milimonfared, and S. H. Fathi, "A review of low-voltage ride-through enhancement methods for permanent magnet synchronous generator based wind turbines," Renew. Sustain. Energy Rev., vol. 47, pp. 399–415, Jul. 2015.

[13] M. Mirhosseini, J. Pou, and V. G. Agelidis, "Single- and two-stage inverter- based grid-connected photovoltaic power plants with ride-through capa- bility under grid faults," in IEEE Trans. Sustain. Energy, vol. 6, no. 3, pp. 1150–1159, Jul. 2015.

[14] M. Castilla, J. Miret, J. L. Sosa, J. Matas, and L. G. de Vicu˜ a, "Grid-fault n control scheme for three-phase photovoltaic converters with adjustable power quality characteristics," IEEE Trans. Power Electron., vol. 25, no. 12, pp. 2930–2940, Dec. 2010.

[15] R. Teodorescu, M. Liserre, and P. Rodreguez, "Control of grid convert- ers under grid faults," in Grid Converters for Photovoltaic and Wind Power Systems, vol. 1. Hoboken, NJ, USA: Wiley, 2011, pp. 237– 287.

[16] S. Mortazavian, M. M. Shabestary, and Y. A.-R. I. Mohamed, "Analysis and dynamic performance improvement of grid-connected voltage-source converters under unbalanced network conditions," in IEEE Trans. Power Electron., vol. PP, no. 99, pp. 1–1, doi: 10.1109/TPEL.2016.2633994.

[17] A. Moawwad, M. S. El Moursi, W. Xiao, and J. L. Kirtley, "Novel con- figuration and transient management control strategy for VSC-HVDC," IEEE Trans. Power Syst., vol. 29, no. 5, pp. 2478–2488, Sep. 2014.

[18] A. Moawwad, M. S. El Moursi, and W. Xiao, "Advanced fault ride-throug management scheme for VSC-HVDC connecting offshore wind farms," IEEE Trans. Power Syst., vol. 31, no. 6, pp. 4923–4934, Nov. 2016.

[19] A. Moawwad, M. S. El Moursi, and W. Xiao, "A novel transient control strategy for VSC-HVDC connecting offshore wind power plant," IEEE Trans. Sustain. Energy, vol. 5, no. 4, pp. 1056–1069, Oct. 2014.

[20] J. Miret, A. Camacho, M. Castilla, L. G. de Vicu˜ a, and J. Matas, "Control n scheme with voltage support capability for distributed generation invert- ers under voltage sags," IEEE Trans. Power Electron., vol. 28, no. 11, pp. 5252–5262, Nov. 2013.

[21] T. Lee, S. Hu, and Y. Chan, "D-STATCOM with positive-sequence ad- mittance and negative-sequence conductance to mitigate voltage fluc- tuations in high-level penetration of distributed generation systems," IEEE Trans. Ind. Electron., vol. 60, no. 4, pp. 1417–1428, Apr. 2013.

[22] M. Castilla, J. Miret, A. Camacho, J. Matas, and L. G. de Vicu˜ a, "Volt- n age support control strategies for static synchronous compensators under unbalanced voltage sags," IEEE Trans. Ind. Electron., vol. 61, no. 2, pp. 808–820, Feb. 2014.

[23] S.-F. Chou, C.-T. Lee, H.-C. Ko, and P.-T. Cheng, "A low-voltage ride through method with transformer flux compensation capability of renew- able power grid-side converters," IEEE Trans. Power Electron., vol. 29, no. 4, pp. 1710–1719, Apr. 2014.

[24] M. M. Shabestary and Y. A. R. I. Mohamed, "An analytical method to obtain maximum allowable grid support by using grid-connected con- verters," IEEE Trans. Sustain. Energy, vol. 7, no. 4, pp. 1558–1571, Oct. 2016.

[25] M. M. Shabestary, A comparative analytical study on low-voltage ride-through reference-current-generation (LVRT-RCG) strategies in converter-interfaced DER Units, Master's thesis, Dept. Electr. Comput. Eng., Univ. of Alberta, Edmonton, AB, Canada, 2015.

[26] M. M. Shabestary and Y. Mohamed, "Analytical expressions for multi- objective optimization of converter-based DG operation during unbal- anced grid conditions," in IEEE Trans. Power Electron., vol. 32, no. 9, pp. 7284–7296, Sep. 2017.